Ion beam technology for space debris mitigation

Claudio Bombardelli
Space Dynamics Group, School of Aerospace Engineering,
Technical University of Madrid
Plaza Cardenal Cisneros, 3
Madrid, 28040
Spain

claudio.bombardelli@upm.es

ABSTRACT

Actively removing existing manmade debris from high-altitude crowded regions in low earth orbit is a necessary step for the sustainability of space. Yet, no active debris removal (ADR) mission has been flown to date and there is still no consensus on the best way to implement large-scale, reliable ADR operations in the future. One way to tackle the formidable technical challenges of such missions is to exploit removal methods not requiring hard mechanical contact with the target. This lecture reviews contactless ion beam actuation as one of such methods. The most critical aspects of this technology are discussed providing fundamental modeling tools to assess its performance and identify its main challenges.

Contents

1.0 INTRODUCTION

After almost 60 years of space activities about 6000 tons of manmade material has been left in Earth orbit in form of active and defunct satellites, rocket upper stages, and fragments of both. More than 40% of this mass accumulated in low earth orbit (LEO), by far the most crowded region around Earth, where the first ever collision between two large satellites in orbit occurred in 2009.

While the good practice of deorbiting newly launched satellites before the end of their operational lifetime will dramatically reduce collision risks it will likely not be enough to stabilize the space debris environment. Studies have pointed out that in order to limit the growth of debris fragments to a sustainable level is will be necessary to deorbit a few ton-class existing space debris per year [1] following a procedure known as Active Debris Removal (ADR). To date, no ADR mission has yet been launched.

Among the different challenges involved with ADR stands the difficulty of delivering the required deorbiting or reorbiting momentum to the target in a reasonable time frame. The most intuitive mean to do that is to have an active spacecraft docking with the debris and performing the required orbit change. Unfortunately, docking to an old non-cooperative object in poorly known conditions and with a possibly tumbling or spinning motion is technologically very complicated and risky. The post-docking challenge of stabilizing and maneuvering a compound object made up by a large debris and a (hopefully small) deorbiting platform should also not be underestimated.

A promising alternative to get around these difficulties is to transfer the momentum remotely using the exhaust of an ion thruster pointed at the target from a nearby shepherd satellite, as it has been proposed in [2]. The concept, originally named “ion beam shepherd” (IBS), would be applicable to asteroid deflection too [3]. The beam would transfer enough momentum to modify the debris orbit from a safe distance in a controlled manner without the need for docking to it. Apart from reducing risk, the technique offers important additional advantages: it works independently of the particular target shape, rotation state or material, it is fully reusable up to complete fuel depletion, it offers full maneuverability of the shepherd spacecraft towards different targets in LEO, and relies on high technology readiness level (TLR) space hardware like conventional ion thrusters.

Although in principle conceptually simple, the proposed removal approach involves new and interesting challenges from the dynamics and control point of view, which need to be addressed in order to maximize its efficiency. Most importantly, the shepherd spacecraft and the space debris should be simultaneously de-orbited (or re-orbited) in a controlled and reliable way, keeping a safe distance between each other to minimize collision risks and contamination. This implies not only the need for advanced sensors, actuators and control strategies, but also the need for accurate models describing the hypersonic ion beam expansion and interaction with the surrounding environment as well as the dynamic interactions between the debris and the plasma beam.

The complexity and multidisciplinary character of the IBS concept recommends the development and employment, as much as possible, of reasonably accurate yet simple analytical models to describe the different physical processes involved. These models are a valid resource for the aerospace engineer dealing with a non-conventional spacecraft design as well as for researchers and scientists seeking to explore new avenues to improve the performance and range of applications of the concept.

The present lecture will introduce the IBS concept, discuss its domain of applications and technological challenges and provide the most updated analytical modeling tools developed in the last six years of research by this author and his collaborators.

2.0 ENVIRONMENTAL CRITICALITY IN LEO

Before considering any candidate ADR technology it is paramount to understand the space debris environment, its current state and evolution and what measures can be taken to improve it.

With regard to the space debris problem, the "fitness" of the space environment is lower the higher the risk for present and future space assets to be hit by uncontrolled manmade objects left in orbit. The biggest threat in this sense is actually represented by the small fragments population of 1-10 cm in size. These fragments, more abundant and therefore more likely to impact an active spacecraft when compared to larger objects, cannot be tracked from the ground but are large enough to fully disable a space asset. Yet the main sources contributing to the growth of these fragments are in-orbit explosions and collisions involving large and massive objects, which should be the primary target of ADR operations. Among the massive ton-class objects left in LEO, what remains to decide is what specific targets should be given priority in the removal process and in what orbits they reside.

In this regard, it is very instructive to look at the two major fragment-generating events in the history of space exploration: the 2009 Cosmos-Iridium collision and the 2007 Fengyun-C anti-satellite missile test. The former, which occurred at about 789 km altitude, is estimated to have 90% of its fragments to reenter the atmosphere by 2024. On the other hand, we will have to wait until about 2090 to have the atmosphere getting rid of the same fraction of fragments for Fengyun-C , generated at about 865 km altitude [4]. This suggests that higher altitude objects pose a much bigger potential threat to the environment and several authors have suggested that ballistic lifetime, together with object mass and local debris population density, should be accounted for in the definition of a criticality index for the individual debris objects (see [5]). The importance of orbital altitude can be appreciated in Fig. 1 where the overall criticality of the LEO region has been evaluated using formulas provided in the previous reference and compared with the overall mass distribution and trackable ($>$10 cm) objects density as a function of the orbital altitude. The region between 950 and 1000 km altitude is by far the most critical and should be the main focus of future ADR activities. Conversely, the 800+ tons of space debris below 750 km have a minor impact on the overall environmental criticality. Studies are ongoing to evaluate the benefit of repositioning large debris in this region as opposed to fully deorbit them to take advantage of the lower delta-V cost of the repositioning operation [6].

3.0 THE ION BEAM SHEPHERD CONCEPT

Ion and plasma thrusters commonly used in space technology propel spacecraft by accelerating plasma ions away and producing reaction forces as a result of Newton's third law of motion. After being accelerated, the expelled plasma ions are released into the environment at a few tens of km/s velocity relative to the spacecraft frame and their kinetic energy can be considered lost. However, if the ions intercept a macroscopic body in

the vicinity of the spacecraft they will enter in the material substrate of the body, lose both their energy and momentum as a result of collisions, and give rise to a force exerted remotely on the body.

The capability of transferring forces between nearby orbiting objects without hard mechanical contact is extremely useful in space technology, which motivates some effort to exploit the previously described interaction in practical terms. A technology implementation of contactless ion beam actuation is depicted in Fig. 2 where a shepherd satellite (S) employs a primary, impulse transfer, thruster (ITT) pointed at a nearby target whose orbit needs to be be modified. In order to make the process work, it is essential to have a secondary, impulse compensation, thruster (ICT) mounted on the shepherd and generating a counteractive force in order to keep it in the vicinity of the target at all times. A small beam divergence allows the shepherd to operate efficiently (i.e. with almost full beam overlap and momentum transmission) at a safe distance from a target body (T). For large size space debris and state-of-the-art technology one can expect separation distances in the 5-15 m range depending on beam divergence and spacecraft guidance navigation and control (GNC) capabilities.

4.0 BEAM MODELING

The core technological element of the IBS concept is its electric propulsion system, and in particular the ITT. Ideally, an ITT should be able to create a low-divergence beam in order to have, for a given target-shepherd distance, the highest possible fraction of its ions hitting the target. In addition to that, it should have a high specific impulse (say >3000 s) and long operational lifetime (a few years), to enable the removal of multiple targets, and a high technology readiness level to minimize uncertainties in the mission cost and schedule. This suggests, at least for the time being, to rely on high-voltage, gridded ion thrusters.

4.1 Thruster equations

One of the most important design parameters in a gridded ion thruster is the beam acceleration voltage V_{beam}, which is approximately equal to the innermost (positive) grid voltage. This voltage determines the effective exhaust speed v_0 of the plasma and hence the specific impulse I_{sp} of the thruster according to (see [7]):

$$I_{sp} = \frac{v_0}{g_0} = \frac{\kappa \cdot \eta_m}{g_0}\sqrt{\frac{2q_e V_{beam}}{m_i}}.$$

In the above equation, $q_e = 1.6 \times 10^{-19}$C is the electric charge of the electron, m_i is the atomic mass of the propellant (for xenon $m_i \simeq 2.18 \times 10^{-25}$kg), g_0 is the sea level gravity acceleration, $\eta_m = \dot{m}_i/\dot{m}$ is the propellant mass utilization efficiency, which determines the propellant fraction coming out of the thruster as ions, and κ is a correction factor, very close to unity, which accounts for the thruster divergence angle and the existence of doubly charged ions. The mass utilization efficiency is an important figure of merit for a thruster also because a higher η_m generally implies a longer lifetime. In general, larger size thrusters tend to offer a higher mass utilization efficiency.

A high beam voltage plays a key role in reducing beam divergence. A perfectly collimated (i.e. parallel) ion beam cannot be obtained due to the non-zero temperature of the plasma ions before being accelerated and to aberration effects in the beam extraction and acceleration process. If one neglects these effects, a minimum theoretically achievable divergence at the thruster exit can be written as a function of the specific impulse and the plasma ion temperature T_i(eV) [8]:

$$\beta_{min} \approx \tan^{-1}\left(\frac{\sqrt{2q_e T_i/m_i}}{I_{sp} g_0}\right),$$

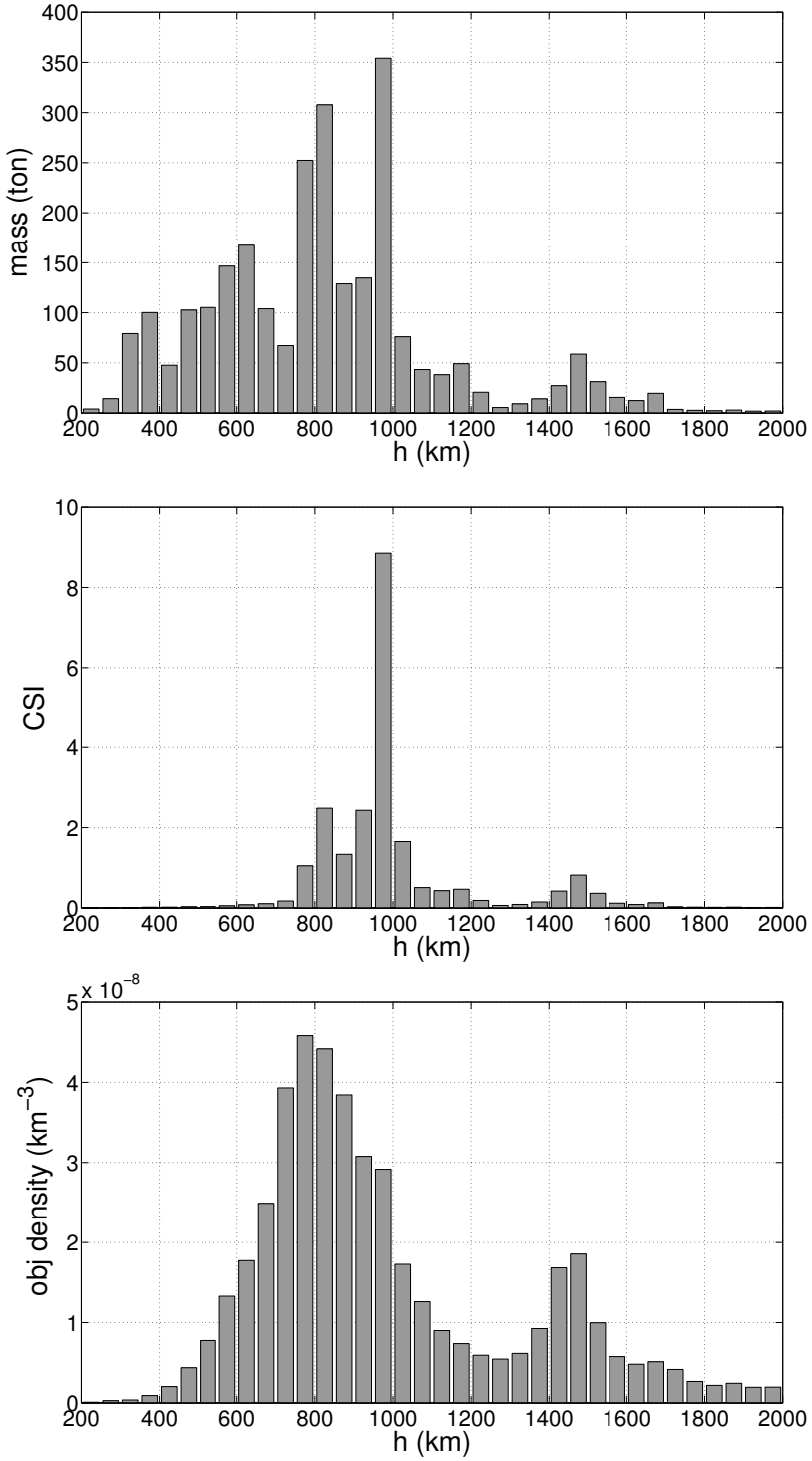

Figure 1: Mass, criticality and trackable object density altitude distribution in LEO

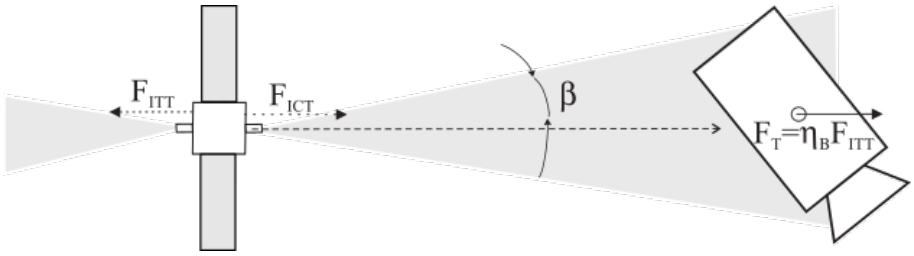

Figure 2: Schematic of ion beam shepherd (IBS).

For a given specific impulse I_{sp} the nominal thrust can be obtained as

$$F_{ITT} = \dot{m} I_{sp} g_0.$$

where the mass flow rate $\dot{m}$ can work as a control parameter to modify the nominal thrust at constant discharge voltage. Another common way of expressing the nominal thrust is through the beam current $I_{beam} = q_e \dot{m}_i / m_i$ as:

$$F_{ITT} = \kappa \sqrt{\frac{2m_i}{q_e}} I_{beam} \sqrt{V_{beam}}.$$

The amount of beam current produced for a given thruster electrical power P_{THR} at a given discharge voltage is related to the thruster electrical efficiency η_e as:

$$\eta_e = \frac{V_{beam} I_{beam}}{P_{THR}}.$$

The overall thruster efficiency:

$$\eta_T = \frac{1}{2} \frac{F_{ITT} I_{sp} g_0}{P_{THR}} = \kappa^2 \eta_m \eta_e$$

measures the fraction of supplied electrical energy effectively converted into useful kinetic energy imparted to a spacecraft.

4.2 Beam expansion and transmitted force

The study of the propagation and expansion of a neutralized ion beam in the vacuum, as relevant to the IBS concept, was pioneered by Parks and Katz [9] in the 70s and revisited by Ashkenazy and Fruchtman [10] in 2001. More recent contributions, directly related to the IBS concept are found in the work of Merino et al. [11] and Cichocki at al. [12].

For the purpose of computing forces and torques transmitted by an ion beam to a target object what needs to be modeled is the 3D profile of the ion density and velocity. The simplest possible way to obtain such distribution is to employ a collisionless fluid model accompanied by a simplified model for the electron temperature. Such model is adequate for a reasonably accurate description of the beam expansion far enough from the thruster, i.e. in the far field of the beam.

In the “cold beam” limit, that is, neglecting electron pressure effects by setting electron temperature equal to zero, the beam expands as a cone with the density distribution following a Gaussian profile in the radial (r)

direction and decaying axially with the square of the distance (z) from the cone vertex:

$$n(r,z) = \frac{3n_0 R_0^2}{\tan^2\beta_0 \cdot z^2} \exp\left(-\frac{3r^2}{\tan^2\beta_0 \cdot z^2}\right). \tag{1}$$

In the above equation the near-field divergence angle β_0 defines the beam radial envelope containing 95% of the total beam current while n_0 is the average density of the beam measured at a reference beam section R_0[1]. The reference density can be related to the nominal ion engine thrust and exhaust velocity by:

$$n_0 = \frac{F_{ITT}}{\pi r_0^2 m_i v_0^2}.$$

The conical velocity distribution in the cold beam limit can be described by the relation:

$$\mathbf{v} = v\mathbf{u}_t \approx v_0\left(\mathbf{u}_z + \frac{r}{z}\mathbf{u}_r\right), \tag{2}$$

where v_0 is the magnitude of the (approximately constant) axial velocity components of the ions and $\mathbf{u}_r, \mathbf{u}_z$ are the radial and axial unit vectors, respectively.

In a more realistic case, non-negligible electron pressure effects will make the beam expand as a funnel. Under the "isothermal beam" hypothesis where electron temperature is considered constant along the beam the local beam divergence β increases logarithmically and can be well approximated with the relation [10]:

$$\tan\beta \approx \sqrt{\tan^2\beta_0 + \epsilon^2 \ln\left(\frac{\epsilon z}{R_0}\right)} \tag{3}$$

where the dimensionless parameter:

$$\epsilon = \frac{12}{M^2} = \frac{12 q_e T_e}{I_{sp}^2 g_0^2 m_i},$$

quantifies the influence of the temperature $T_e\,(\mathrm{eV})$ of the beam neutralizing electrons (with Mach number M) on the far-field beam divergence and underlines the beneficial influence of a high specific impulse in reducing the divergence increase.

After identifying with Σ the surface, with local normal $\mathbf{u}_n$, intercepted by the beam streamlines with velocity $\mathbf{v}$ and local density n, the force transmitted by the beam to an object of generic shape can be obtained by the integral:

$$\boldsymbol{F}_B = \int_\Sigma m_i n \mathbf{v}\,(\mathbf{v}\cdot\mathbf{u}_n)\,dS,$$

or, equivalently:

$$\boldsymbol{F}_B = \frac{3F_{ITT}}{\pi\tan^2\beta}\int_\Sigma \exp\left(-\frac{3r^2}{\tan^2\beta\, z^2}\right)\frac{\mathbf{u}_t\,(\mathbf{u}_t\cdot\mathbf{u}_n)}{z^2}dS. \tag{4}$$

In general, the above integral is to be evaluated numerically and the logarithmical increase in divergence (Eq. (3)) should be taken into account for an accurate force estimation. On the other hand, the streamline

[1] it is convenient to consider R_0 as the corresponding beam cross section where the near field divergence is experimentally measured. This is typically done at around 2 thruster radii from the thruster exit, where near-field effects have decayed and the beam profile is nearly Gaussian.

direction unit vector $\mathbf{u}_t$ can be well approximated by the conical field equation (2) with negligible error. This fact is important because it allows one to employ very efficient projection methods to calculate the above integral as proposed by Alpatov et al. [13].

Once the force transmitted by the beam is computed one can derive the *beam momentum transfer efficiency*, a fundamental figure of merit defined as the ratio between the beam force component along the beam axis and the nominal ITT thrust:

$$\eta_B = \frac{\boldsymbol{F}_B \cdot \mathbf{u}_z}{F_{ITT}}.$$

4.3 Cannonball model

A very useful simplification for the computation of the transmitted force to an object immersed in an ion beam is to regard the object as a perfect sphere, which permits the derivation of important analytical relations employed for preliminary design purposes as well as to investigate the dynamics and control of a shepherd-target formation in orbit.

Let us consider a spherical target of radius R_T. From now on all length quantities will be written in non-dimensional form using R_T as reference length, unless indicated otherwise. Let the geometrical center of the target be located at a distance δ from the beam vertex with an angular offset α from the beam axis (see Fig. 3).

The force transmitted to the sphere can be obtained through Eq. (4) where the surface of integration Σ is the base of the spherical cap of radius $\hat{R}$ delimited by the beam envelope (as in Fig. 3) and having normal unit vector $\mathbf{u}_n = \mathbf{u}_r \sin\alpha + \mathbf{u}_z \cos\alpha$ and in-plane tangential unit vector $\mathbf{u}_\theta = \mathbf{u}_r \cos\alpha - \mathbf{u}_z \sin\alpha$. Due to the axial symmetry of the beam the resulting force can be decomposed along these two directions and has zero out-of-plane component:

$$F_n = \boldsymbol{F}_B \cdot \mathbf{u}_n$$

$$F_\theta = \boldsymbol{F}_B \cdot \mathbf{u}_\theta$$

A generic point P belonging to Σ has radial and axial coordinates:

$$r_P = \sqrt{(s\ \sin\phi)^2 + (d\ \sin\alpha - s\ \cos\alpha\cos\phi)^2}$$

$$z_P = d\ \cos\alpha - s\ \sin\alpha\cos\phi$$

where $0 < s < \hat{R}$, $0 < \phi < 2\pi$ and d is the distance of the center of Σ from the beam vertex with:

$$d = \delta - \frac{1}{\delta}, \qquad \hat{R} = \sqrt{1 - \frac{1}{\delta^2}}.$$

After substituting the preceding expressions for r_P, z_P into Eq. (4) together with the conical velocity field relation (2) one obtains the non-dimensional force components along the normal and transversal directions as:

$$f_n = \frac{F_n}{F_{ITT}} = \frac{3d^2}{\pi\tan^2\beta}\int_0^{2\pi}\int_0^{\hat{R}} \frac{1}{z_P^4}\exp\left(-\frac{3r_P^2}{\tan^2\beta\, z_P^2}\right) ds d\phi,$$

$$f_\theta = \frac{F_\theta}{F_{ITT}} = \frac{3d}{\pi \tan^2 \beta} \int_0^{2\pi} \int_0^{\hat{R}} \frac{s^2 \cos\phi}{z_P^4} \exp\left(-\frac{3r_P^2}{\tan^2 \beta \, z_P^2}\right) ds d\phi.$$

Finally, the dimensionless beam force can be written as:

$$\boldsymbol{f}_B = f_r \mathbf{u}_r + f_z \mathbf{u}_z,$$

with:

$$f_r = f_n \cos\alpha - f_\theta \sin\alpha$$

$$f_z = f_n \sin\alpha + f_\theta \cos\alpha.$$

The preceding integrals are not solvable in closed analytical form. Nevertheless, a small angle approximation exists in the form:

$$f_r = f_{r,1}\alpha + \mathcal{O}\left(\alpha^3\right) \tag{5}$$

$$f_z = \eta_B + f_{z,2}\alpha^2 + \mathcal{O}\left(\alpha^4\right). \tag{6}$$

where the beam momentum transfer efficiency for a spherical target whose center is located on the beam axis at a distance of δ target radii from the vertex of the beam has the compact expression:

$$\eta_B = 1 - \exp\left[-\frac{3}{\tan^2 \beta \left(\delta^2 - 1\right)}\right], \tag{7}$$

and where:

$$f_{r,1} = \frac{3\delta^2 \left(1 - \eta_B\right)}{\tan^2 \beta \left(\delta^2 - 1\right)^2}, \tag{8}$$

$$f_{z,2} = \frac{9\delta^2 \left(1 - \eta_B\right)\left[\tan^2 \beta \left(\delta^2 - 1\right) - 2\delta^2\right]}{2 \tan^2 \beta \left(\delta^2 - 1\right)^3}. \tag{9}$$

Eq. (7) can be easily inverted to determine the separation distance corresponding to a given momentum transfer efficiency:

$$\delta\left(\eta_B\right) = \sqrt{1 - \frac{3}{\tan^2 \beta \ln\left(1 - \eta_B\right)}}. \tag{10}$$

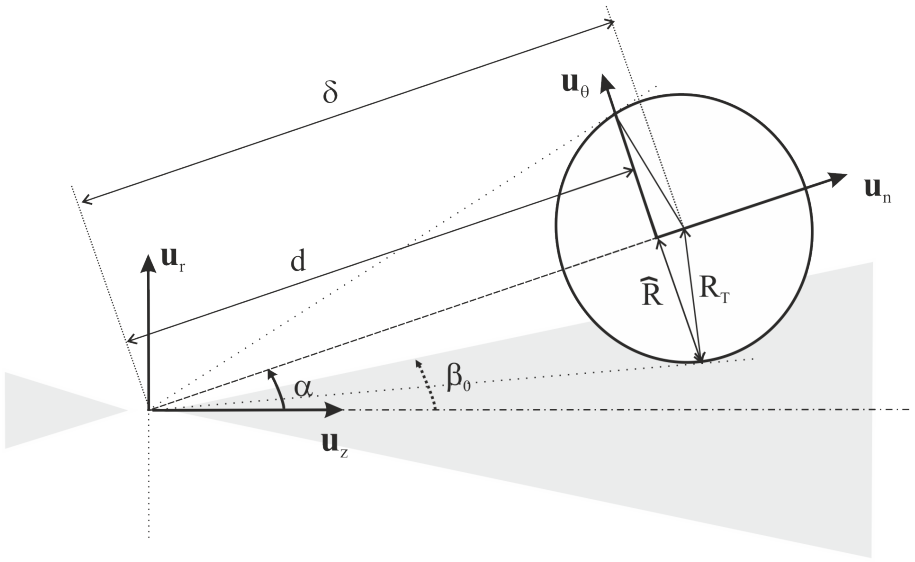

Figure 3: Cannonball model beam-target geometry

4.4 Beam gradient matrix

Of interest for the dynamics and control of the target-shepherd relative position is the dimensionless beam gradient matrix. The latter is here defined as the gradient of the beam force vector $\boldsymbol{f}_B$ when the target center of mass lays on a nominal controlled position $\boldsymbol{\delta}_0$:

$$\boldsymbol{\Gamma}_B = \left. \frac{d\boldsymbol{f}_B}{d\boldsymbol{\delta}} \right|_{\boldsymbol{\delta}=\boldsymbol{\delta}_0},$$

For a spherical target whose center of mass and geometrical center coincide (zero-offset sphere) and are located on the beam axis at distance δ from the center of the beam ($\boldsymbol{\delta}_0 = \delta \mathbf{u}_z$), the beam gradient matrix expressed in a Cartesian reference system centered at the beam cone vertex with z along the beam axis, x normal to the plane containing the beam axis and the sphere center, and y following the right-hand rule can be obtained from Eqs. (5-9) after noting that:

$$\frac{\partial f_z}{\partial z} = \frac{\partial f_z}{\partial \delta},$$

$$\frac{\partial f_x}{\partial x} = \frac{\partial f_y}{\partial y} = \frac{1}{\delta}\frac{\partial f_r}{\partial \alpha},$$

finally leading to:

$$\boldsymbol{\Gamma}_B = \begin{bmatrix} b & 0 & 0 \\ 0 & b & 0 \\ 0 & 0 & -2b \end{bmatrix},$$

with:

$$b = \frac{3\delta\left(1-\eta_B\right)}{\tan^2\beta\left(\delta^2-1\right)^2}.$$

The function b tends to zero for $\delta \to 0$ (i.e. $\eta_B \to 1$) and for $\delta \to \infty$. It is maximum for:

$$\delta = \tilde{\delta} = \frac{\sqrt{3 + \sqrt{9 + \tan^2 \beta}}}{\tan \beta},$$

corresponding to a momentum transfer efficiency of about 40%, where the beam gradient reaches:

$$b_{max} \approx \frac{\sqrt{6}}{2\sqrt{e} \tan \beta}.$$

5.0 ION BEAM MATERIAL INTERACTION

The force transmitted to an object irradiated by an ion beam comes from the transmitted angular momentum of the impinging ions typically at hundreds to a few thousands electron-volt energy, which penetrate the material substrate until they completely stop as a results of elastic and inelastic collisions. Fast ions penetrating solids lose energy by elastic collisions with the target nuclei (nuclear stopping) and by inelastic ionizations and excitation (electronic stopping). It is important to stress than the probability of having an incident ion "bouncing back" instead of penetrating the material substrate is practically zero unless the beam ions strike the surface at grazing incidence. Even in that case the percentage of backscattered ions is still very small. What is emitted from the surface of the object is, instead, a flow of back-sputtered atoms or clusters of atoms belonging to the target material itself.

The momentum of the back-sputtered material has a negligible contribution to the force transmission mechanism because the atoms are emitted with energy of typically two orders of magnitude smaller than the incident ions. Nevertheless, the sputtering process has an important consequence for the IBS concept as it may lead to dangerous contamination levels of sensitive surfaces on the shepherd spacecraft.

5.1 Sputtering

Physical sputtering is an atomic scale process that can occur if an incident particle can transfer sufficient energy to a surface or bulk target atom to overcome its bulk displacement energy and/or its surface binding energy. The energy is transferred through a collisional mechanism by electronic and nuclear collisions and can occur in three regimes for growing energy and mass of the incident ions: the single knock-on, the linear cascade and the spike regime. The first regime operates when the energy transferred from the incident particle to target atoms is only enough to produce one or two knock-ons. This is the case of sputtering with low-energy and/or light ions. Sputtering in this regime cannot be well described using conventional models. The second regime, linear-cascade, is considered when collisions between the impinging particle and target atoms give rise to displacement cascades, but only a small fraction of atoms within the cascade volume are set in motion. Here, the cascade can be visualized as a series of binary collisions between a moving and a stationary atom. The collisional phase of these cascades can be well described by transport equations. Sputtering in the linear-cascade regime was theoretically treated in most detail by Sigmund [14]. For bombardment with high-energy, heavy ions or with molecular ions, the density of recoil atoms within the cascade is so high that encounters between moving atoms become frequent events, the linearity assumption is no longer satisfied, and the third regime, spike, becomes important. For the ion energies and masses characterizing IBS applications a linear cascade sputtering regime is to be expected.

The erosion due to physical sputtering is quantified by the *sputtering yield*, Y, a statistical variable defined as the mean number of atoms removed from a solid target per incident ion. The sputtering yield depends

on a number of factors including the energy of the incident ions, the atomic masses of both incident and target material and the ions' angle of incidence. Several analytical, semi-analytical and numerical sputtering models have been proposed in the literature. The major tool used to understand sputtering and to calculate the sputtering yield Y is Sigmund's linear-cascade theory, which predicts a linear dependence of the sputtering yield (at normal incidence) Y:

$$Y(E) = \frac{x_0}{\pi^2 U}\mathcal{F}_D,$$

In the preceding equation, U is the surface binding energy of the target material, x_0 is the effective depth of origin of the sputtered atoms (typically around 0.5 nm). The surface deposited energy density $\mathcal{F}_D$, depends upon type, energy, and incident angle of the beam ions, and on additional target parameters (e.g., temperature), and can be factorized as:

$$\mathcal{F}_D = \alpha_M N S_n(E).$$

In the preceding equation, α_M is a quantity depending primarily on the ratio M_2/M_1 of the projectile to target mass and can be approximated by:

$$\alpha_M \approx 0.3\,(M_2/M_1)^{2/3}\,.$$

The remaining terms N and S_n are, respectively, the number of target atoms per volume and the nuclear stopping cross section. The latter strongly depends on the energy (E) of the ion beam and can be evaluated experimentally or with empirical models, such as the one proposed by [15] and [16].

A last very important aspect concerning the sputtering process is its dependency with the direction of the incident ion beam with respect to the target normal direction. For not too large an incident angle (θ) the ratio between the actual yield and the zero-incidence yield obeys:

$$\frac{Y\,(E,\theta)}{Y\,(E,0)} \approx \cos\,(\theta)^{-\mu_M}$$

where μ_M is a function of the projectile/target mass ratio and becomes approximately unity for $M_2/M_1 > 5$. Note that the above expression cannot be used to provide the incidence angle corresponding to maximum sputtering, which is very oblique (around 60-70 degrees).

The *differential sputtering yield*, $y\,(\varphi,\psi)$, describes the number of sputtered atoms per incident ion and per solid angle that end up traveling away from the surface in a particular direction. Differential sputtering yields have units of atoms/ions/sr and are functions of both the polar (φ) and azimuthal (ψ) angle of the ejected material. Knowing the differential sputtering yield is important for estimating the re-deposited material, like in the IBS concept. In general the angular dependence is complex and its estimation through analytical models (see for instance [17]) should be supported by experimental data whenever possible.

5.2 Back-sputtering Contamination

Back sputtered atoms or molecules that intercept the shepherd spacecraft will produce molecular contamination. Among the contamination-sensitive spacecraft elements the most critical for an IBS are typically the large solar panels required to power the electric propulsion system. The recommended thickness limit for (photochemically deposited) contamination layer on solar arrays is 0.015 mm leading to a power loss of roughly 2% [18]. Thermal control surfaces and (single-surface) visible sensors are less critical and can tolerate a 0.2 mm

contamination thickness. Infrared sensors, like LIDARs, are even less critical and would experience a 10% decrease in absorption only after a deposited thickness of about 1.5 mm [18].

Apart from employing appropriate design margins (e.g. higher power budget margins to compensate for solar panels degradation) the best way to mitigate the contamination issue is to increase the target-shepherd separation distance as much as possible (the amount of contamination reaching the shepherd depends roughly on the square of that distance). In order not to compromise momentum transfer efficiency this will be possible only by reducing beam divergence, which is perhaps the most beneficial technological advance for the IBS concept in the future.

6.0 MISSION DESIGN

6.1 Thruster sizing

The most efficient way to change the orbit of a target debris with an IBS is to have the shepherd in a coorbiting formation with the target, that is with the same osculating orbital elements except for a small separation in true anomaly, and with both its thrusters pushing nominally along the instantaneous orbital velocity thereby transmitting a tangential beam force to the target.

If the target eccentricity is small, as it is the case for the great majority of LEO space debris, and the formation is controlled in such a way that no differences in semi-major axes arise, the nominal target-shepherd separation distance remains approximately constant[2]. The need to have both objects evolving with the same semi-major axis sets a constraint for the nominal operation point of the ITT and ICT propulsion system on the shepherd. After denoting with m_S and m_T the shepherd and target mass respectively, the constraint reads:

$$\frac{F_{ICT} - F_{ITT}}{m_S} = \eta_B \frac{F_{ITT}}{F_{ICT}},$$

resulting in:

$$F_{ICT} = \left(1 + \frac{m_S}{m_T}\eta_B\right) F_{ITT} = \rho_{th} F_{ITT},$$

where $\rho_{th} > 1$ is the thrust magnitude ratio. Note that the fulfillment of the preceding constraint, which is not obvious given the uncertainty on the actual target mass and shape, can be obtained by adjusting three independent quantities: the two thruster magnitudes and the separation distance, which affects η_B. Nevertheless, a minimum η_B will likely be required by mission constraints while the operational regime of the ITT may be set around an optimized design point, leaving the ICT thrust as the most suitable parameter for adjusting the nominal formation geometry.

Under the hypothesis of small orbit eccentricity throughout the deorbiting process one can relate the required ITT thrust magnitude to the desired instantaneous altitude descent/ascent rate $\dot{h}$ by the simple relation valid for quasi-circular orbit evolution under tangential thrust:

$$F_{ITT} \simeq \frac{\pi m_T \left|\dot{h}\right|}{\eta_B T_{orb}},$$

where T_{orb} is the orbital period (95-110 min in LEO, depending on the altitude of interest).

[2] in a coorbiting formation the separation distance is maintained constant except for a periodic fluctuation equal to the separation distance multiplied by the orbit eccentricity

The power needed by the propulsion system obeys:

$$P_{PS} = \frac{g_0}{2\eta_{PPU}} \left[\left(\frac{FI_{sp}}{\eta_T} \right)_{ITT} + \left(\frac{FI_{sp}}{\eta_T} \right)_{ICT} \right],$$

where η_{PPU} is the power and propulsion unit (PPU) conversion efficiency. The above relation can be written in a more convenient form by assuming equal specific impulse and thrust efficiency for both thrusters[3], in which case one has:

$$P_{PS} \approx \frac{\pi I_{sp} g_0 m_{eq} \left| \dot{h} \right|}{2\eta_{PPU}\eta_T T_{orb}},$$

where m_{eq} is the formation equivalent mass:

$$m_{eq} = m_S + 2\frac{m_T}{\eta_B}.$$

Finally the overall propellant consumption over the total thrust time Δt can be computed as:

$$m_f = \left[\left(\frac{F}{I_{sp} g_0} \right)_{ITT} + \left(\frac{F}{I_{sp} g_0} \right)_{ICT} \right] \Delta t + m_{f,RCS},$$

where $m_{f,RCS}$ is the fuel spent by the reaction and control system to maintain the coorbiting formation throughout the mission. Assuming again equal specific impulses and efficiencies for the two main thrusters we have:

$$m_f \approx \frac{\pi m_{eq} \Delta h}{T_{orb} I_{sp} g_0} + m_{f,RCS},$$

where Δh is the overall altitude ascent/descent range.

The total mass of the shepherd spacecraft can finally be estimated as:

$$m_S = \alpha_P \left(P_{PS} + P_0 \right) + m_f + m_{str}.$$

where α_P is the inverse specific power, P_0 is the power required for other spacecraft subsystems (e.g. thermal control), and m_{str} the spacecraft structure mass.

As an example one can consider a repositioning mission to move Envisat (m_T= 8050 kg T_{orb}= 100 min) by 50 km down in 4 months in order to reduce its environmental criticality. Assuming a 25 meters nominal separation distance (given the particularly complex target shape) corresponding to an average η_B of 50% a specific impulse of 3000 s for both thrusters, a total thrust period of 2.8 months due to a 30% eclipse fraction a PPU thruster efficiency $\eta_{PPU}\eta_T$= 60%, an inverse specific power of 15 kg/kW would result in a 3 kW power requirement for the propulsion system a total 28 kg of Xenon spent. After adding one extra kW of power, 10 kg of RCS fuel and a 150 kg of structure one would obtain a final spacecraft mass of about 350 kg broken down into 38 kg of fuel, 60 kg of power, 150 kg of structure and 100 kg of margins.

[3] in a real mission design one would likely end up with a relatively high specific impulse for the ITT, for minimizing beam divergence, and a lower specific impulse for the ICT in order to reduce power requirements (see [19]).

6.2 Full relative motion equations

The capability of obtaining a stable, low-risk, fully autonomous, prolonged formation flying between the shepherd spacecraft and the target debris is one of the key technology challenges of the IBS concept and requires a full understanding of the relative motion dynamics and the role played by the ion beam force. The main governing equations are derived in the following.

After linearizing the local gravitational field around the shepherd orbital position $\boldsymbol{r}_S$, the equations of motion governing the evolution of the debris relative position $\boldsymbol{\rho} = \boldsymbol{r}_T - \boldsymbol{r}_S$ with respect to the shepherd in a local orbital frame are the Tschauner-Hempel equations as used in [20] with an added perturbing term coming from the differential ion beam acceleration:

$$\ddot{\boldsymbol{\rho}} + \left(\boldsymbol{\Omega}^2 + \dot{\boldsymbol{\Omega}} - \boldsymbol{G}\right)\boldsymbol{\rho} + 2\boldsymbol{\Omega}\dot{\boldsymbol{\rho}} = \frac{\boldsymbol{F}_T}{m_T} - \frac{\boldsymbol{F}_S}{m_S}, \tag{11}$$

where $\boldsymbol{\Omega}$ is the angular velocity matrix of the local orbital frame, $\boldsymbol{G}$ the gravity gradient matrix at the local shepherd position, and $\boldsymbol{F}_T$,$\boldsymbol{F}_S$ the resulting thruster forces on the target and shepherd, respectively.

The preceding equations need to be accompanied by the shepherd orbit evolution written in inertial axes:

$$\ddot{\boldsymbol{r}}_S = -\mu\frac{\boldsymbol{r}_S}{r_S^3} + \frac{\boldsymbol{F}_S}{m_S}.$$

In general, the beam force transmitted to the target depends on the instantaneous attitude of the target with respect to the beam so that the above equations are coupled to the attitude motion equations of the target written in target body axes. After denoting with $\boldsymbol{\mathcal{I}}$ the target inertia tensor, $\boldsymbol{\omega}$ its angular velocity and $\boldsymbol{N}_T$ the resulting torque we have:

$$\boldsymbol{\mathcal{I}}\dot{\boldsymbol{\omega}} + \boldsymbol{\omega} \times (\boldsymbol{\mathcal{I}}\boldsymbol{\omega}) = \boldsymbol{N}_T.$$

6.3 Relative motion equations in quasi-circular orbit

In order to gain insight into the complex relative dynamics of the IBS-target system it is convenient to start off with the simplest possible model. To this end we introduce the following assumptions:

1. The target is modeled as a sphere whose center of mass and geometrical center coincide (zero-offset sphere).

2. The orbits of the IBS and the target are considered quasi-circular.

3. The ion beam is constantly pointed along the shepherd instantaneous velocity vector and opposite to it (deorbiting case), has constant intensity (i.e. the thruster force is constant), and transmits to the debris a force, which only depends on the debris center of mass location relative to the shepherd. Additional thrusters in the three directions can be used to control the position of the IBS but do not affect the target dynamics (i.e. they are not pointed against the target) and their influence on the instantaneous orbit is negligible.

4. All external perturbations are neglected with the exception of the ion beam force.

If the target orbit evolves in a quasi-circular manner Eqs. (11) can be well approximated by the perturbed Clohessy-Wiltshire equations. With respect to a reference frame with the y axis opposite to the instantaneous velocity vector and z opposite to the instantaneous angular momentum[4] vector these equations yield:

$$\begin{cases} \ddot{x} + 2\Omega\dot{y} - 3\Omega^2 x = \dfrac{F_{T,x}}{m_T} - \dfrac{F_{S,x}}{m_S} \\ \ddot{y} - 2\Omega\dot{x} = \dfrac{F_{T,y}}{m_T} - \dfrac{F_{S,y}}{m_S} \\ \ddot{z} + \Omega^2 z = \dfrac{F_{T,z}}{m_T} - \dfrac{F_{S,z}}{m_S} \end{cases} \tag{12}$$

where Ω is the time-varying orbit mean motion. In the above equations the Euler acceleration terms have been neglected since $\dot{\Omega} \ll \Omega^2$ for slow deorbiting.

Let us know linearize the beam force around the nominal equilibrium configuration:

$$\boldsymbol{\rho}_0 = (0, \rho_0, 0)^T \qquad \boldsymbol{F}_{T,0} = (0, F_0, 0)^T \qquad \boldsymbol{F}_{S,0} = \left(0, \frac{m_S}{m_T} F_0, 0\right)^T,$$

where:

$$F_0 = \eta_B F_{ITT},$$

to express:

$$\boldsymbol{F}_T \approx \boldsymbol{F}_{T,0} + \frac{F_0}{R_T} \boldsymbol{\Gamma}_B \left(\boldsymbol{\rho} - \boldsymbol{\rho}_0\right) = \boldsymbol{F}_{T,0} + \frac{bF_0}{R_T} \left[x, -2\left(y - \rho_0\right), z\right]^T.$$

Substituting the preceding relations into Eqs. (12) we get:

$$\begin{cases} \ddot{x} + 2\Omega\dot{y} - 3\Omega^2 x = \dfrac{bF_0}{m_T R_T} x \\ \ddot{y} - 2\Omega\dot{x} = -\dfrac{2bF_0}{m_T R_T} \left(y - \rho_0\right) \\ \ddot{z} + \Omega^2 z = \dfrac{bF_0}{m_T R_T} z \end{cases} \tag{13}$$

Finally, by employing the dimensionless time $\tau = \Omega t$ and introducing the dimensionless target offset components:

$$\xi = \frac{x}{R_T}, \qquad \eta = \frac{y - \rho_0}{R_T}, \qquad \zeta = \frac{z}{R_T},$$

we obtain:

$$\begin{cases} \xi'' + 2\eta' - (3 + \gamma)\,\xi = 0 \\ \eta'' - 2\xi' + 2\gamma\eta = 0 \\ \zeta'' + (1 - \gamma)\,\zeta = 0 \end{cases}, \tag{14}$$

where primes indicate derivatives with respect to the dimensionless time and where we have introduced the dimensionless stiffness coefficient of the beam-target interaction:

[4]Note that, in order to be consistent with the classical orbital mechanics convention, now the y axis is along the ion beam direction, unlike in the previous section

$$\gamma = \frac{b\eta_B F_{ITT}}{m_T \Omega^2 R_T} > 0.$$

The parameter γ is the ratio of a beam gradient over a gravity gradient term and is crucial in order to assess the importance of the beam perturbation on the relative orbit dynamics. Based on the value of γ one can distinguish between a gravity-gradient-dominated ($\gamma \ll 1$), a beam-dominated ($\gamma \gg 1$) and an intermediate regime ($\gamma \sim 1$). Beam-perturbed relative motion in LEO is typically gravity-gradient-dominated.

6.4 Relative motion stability

Eqs. (14) can be rewritten in compact form introducing the state vector $\mathbf{s} = (\xi, \eta, \zeta, \xi', \eta', \zeta')^T$.

$$\mathbf{s}' = \begin{bmatrix} \mathbf{0} & \mathbf{I} \\ -\mathbf{K} & -\mathbf{C} \end{bmatrix} \mathbf{s}$$

where $\mathbf{0}$, $\mathbf{I}$, $\mathbf{K}$,$\mathbf{C}$, are, respectively, the 3×3 null, identity, stiffness and Coriolis gyroscopic matrix, with:

$$\mathbf{K} = \begin{bmatrix} -3-\gamma & 0 & 0 \\ 0 & 2\gamma & 0 \\ 0 & 0 & 1-\gamma \end{bmatrix},$$

$$\mathbf{C} = \begin{bmatrix} 0 & 2 & 0 \\ -2 & 0 & 0 \\ 0 & 0 & 0 \end{bmatrix},$$

The corresponding characteristic polynomial reads:

$$P(\lambda) = P_{out}(\lambda)\, P_{in}(\lambda)$$

with:

$$P_{in}(\lambda) = \lambda^4 + (1+\gamma)\lambda^2 - 2\gamma(3+\gamma)$$

$$P_{out}(\lambda) = \lambda^2 + 1 - \gamma$$

Owing to the problem symmetry the in- and out-of-plane dynamics are decoupled. The latter remain stable if $\gamma < 1$ which means that the radial beam gradient force should not prevail against the gravity gradient restoring force in the direction normal to the orbit plane. On the other hand, as it can be readily verified given the constraint $\gamma > 0$, the open-loop in-plane dynamics are always unstable even for zero beam gradient force.

6.5 Relative motion control

For the purpose of the present analysis we will make the main simplifying assumption that the relative position between the debris and the shepherd center of mass can be estimated at all times with no error. While the assumption is clearly not realistic, as the relative position measurements are a critical aspect of the concept, it allows to focus directly on the control part of the problem. Likewise, as far as the dynamical model employed, we will consider it fully deterministic and obeying to the previously derived equations.

The most straightforward way to control the shepherd-target relative motion is to employ a three-axis thruster-based proportional derivative (PD) feedback control system that acts on the shepherd according to a measured position and velocity deviation with respect to the nominal equilibrium configuration according to:

$$\begin{cases} F_{C,x} = K_{RP}x + K_{RD}\dot{x} \\ F_{C,y} = K_{VP}\left(y - \rho_0\right) + K_{VD}\dot{y} \\ F_{C,z} = K_{HP}z + K_{HD}\dot{z} \end{cases}, \tag{15}$$

After adding the control forces to Eqs.(12) one obtains the full dimensional equations:

$$\begin{cases} \ddot{x} + 2\Omega\dot{y} + \dfrac{K_{RD}}{m_S}\dot{x} + \left(\dfrac{K_{RP}}{m_S} - 3\Omega^2 - \dfrac{bF_0}{m_T R_T}\right)x = 0 \\ \ddot{y} - 2\Omega\dot{x} + \dfrac{K_{VD}}{m_S}\dot{y} + \left(\dfrac{K_{VP}}{m_S} + \dfrac{2bF_0}{m_T R_T}\right)(y - \rho_0) = 0 \\ \ddot{z} + \dfrac{K_{HD}}{m_S}\dot{z} + \left(\dfrac{K_{HP}}{m_S} + \Omega^2 - \dfrac{bF_0}{m_T R_T}\right)z = 0 \end{cases} \tag{16}$$

In this way the new dimensionless stiffness and gyroscopic matrices become:

$$\tilde{\mathbf{K}} = \begin{bmatrix} -3 - \gamma + \gamma_R & 0 & 0 \\ 0 & 2\gamma + \gamma_V & 0 \\ 0 & 0 & 1 - \gamma + \gamma_H \end{bmatrix},$$

$$\tilde{\mathbf{C}} = \begin{bmatrix} \sigma_R & 2 & 0 \\ -2 & \sigma_V & 0 \\ 0 & 0 & \sigma_H \end{bmatrix},$$

with:

$$\gamma_R = \frac{K_{RP}}{m_S\Omega^2}, \qquad \gamma_V = \frac{K_{VP}}{m_S\Omega^2}, \qquad \gamma_H = \frac{K_{HP}}{m_S\Omega^2}$$

$$\sigma_R = \frac{K_{RD}}{m_S\Omega}, \qquad \sigma_V = \frac{K_{VD}}{m_S\Omega}, \qquad \sigma_H = \frac{K_{HD}}{m_S\Omega}$$

After computing the new characteristic polynomial one obtains the stability conditions (to be simultaneously satisfied) for the out-of-plane dynamics:

$$\gamma_H \geq \gamma - 1, \qquad \sigma_H \geq 0$$

and for the in-plane dynamics:

$$\gamma_R \geq \gamma + 3, \qquad \gamma_V \geq -2\gamma, \qquad \sigma_R \geq 0, \qquad \sigma_V \geq 0.$$

Now that the boundary of the stable region are defined one needs to choose proper values of the different dimensionless gains based on some optimization criterion. Instead of following the common procedure of linear quadratic regulator (LQR) control design we can opt for a more straightforward pole-placing approach in which the oscillatory part of the linear response is set to zero. To this end we impose:

$$P_{in}\left(\lambda\right) = \left(\lambda + m^2\right)^4 \quad m \in \mathbb{R}$$

$$P_{out}(\lambda) = \left(\lambda + m^2\right)^2 \quad m \in \mathbb{R}$$

which constrains the choice of the dimensionless control gains to:

$$\gamma_R^* = 3 + \gamma + m^4, \qquad \gamma_V^* = 2\gamma + m^4, \qquad \gamma_H^* = \gamma - 1 + m^4,$$

$$\sigma_R^* = 2 + 2m^2, \qquad \sigma_V^* = -2 + 2m^2, \qquad \sigma_H^* = 2m^2.$$

The proposed control strategy has been studied extensively and shown to offer excellent results even under non-nominal conditions corresponding to targets of irregular shapes and moderately eccentric orbits.

7.0 CONCLUSIONS

An overview of contactless ion beam actuation for space debris removal application has been presented including the most critical aspects of the concepts, starting from the basic concept description and going through the modeling of the different physical phenomena involved. The material should serve as an introduction for the non-experts providing key elements to evaluate the range of application of the method as well as its performance and compare it with other solutions. In addition, it can be the starting point for researchers and scientists to investigate particular aspects in more details. This may hopefully contribute to the further development of a concept that is still relatively young and whose capability has not yet been fully explored.

8.0 ACKNOWLEDGEMENTS

Most of the technical content of this lecture is the result of more than six years of research activity funded by several institutions. We acknowledge funding from the European Union through the FP7 LEOSWEEP project (GA 607457), the STARDUST ITN (GA 317185), The European Space Agency through several research contracts including, among others, the Ariadna and SysNova programs, and the Spanish Ministry of Economy and Competitiveness through research contract ESP2013-41634-P.

REFERENCES

[1] Liou, J.-C., "An active debris removal parametric study for LEO environment remediation," *Advances in Space Research*, Vol. 47, No. 11, 2011, pp. 1865–1876.

[2] Bombardelli, C. and Pelaez, J., "Ion beam shepherd for contactless space debris removal," *Journal of Guidance, Control, and Dynamics*, Vol. 34, No. 3, 2011, pp. 916–920.

[3] Bombardelli, C. and Peláez, J., "Ion beam shepherd for asteroid deflection," *Journal of Guidance, Control, and Dynamics*, Vol. 34, No. 4, 2011, pp. 1270–1272.

[4] Pardini, C. and Anselmo, L., "Physical properties and long-term evolution of the debris clouds produced by two catastrophic collisions in Earth orbit," *Advances in Space Research*, Vol. 48, No. 3, 2011, pp. 557–569.

[5] Rossi, A., Valsecchi, G., and Alessi, E., "The Criticality of Spacecraft Index," *Advances in Space Research*, Vol. 56, No. 3, 2015, pp. 449–460.

[6] Bombardelli, C., Alessi, E. M., Rossi, A., and Valsecchi, G. B., "Environmental Impact of Space Debris Repositioning," *67th International Astronautical Congress, IAC-16*, 2016.

[7] Goebel, D. M. and Katz, I., *Fundamentals of electric propulsion: ion and Hall thrusters*, Vol. 1, John Wiley & Sons, 2008.

[8] Reiser, M., *Theory and design of charged particle beams*, Wiley, New York, 2008, Series in Beam Physics and Accelerator Technology, chapter 3, pp. 56-66.

[9] Parks, D. and Katz, I., "A preliminary model of ion beam neutralization," *AIAA Pap.;(United States)*, Vol. 79, No. CONF-791046-, 1979.

[10] Ashkenazy, J. and Fruchtman, A., "Plasma plume far field analysis," *27th International Electric Propulsion Conference*, 2001.

[11] Merino, M., Cichocki, F., and Ahedo, E., "A collisionless plasma thruster plume expansion model," *Plasma Sources Science and Technology*, Vol. 24, No. 3, 2015, pp. 035006.

[12] Cichocki, F., Merino, M., Ahedo, E., Hu, Y., and Wang, J., "Fluid vs PIC Modeling of a Plasma Plume Expansion," 2015, Joint Conference of 30th International Symposium on Space Technology and Science 34th International Electric Propulsion Conference and 6th Nano-satellite Symposium, Hyogo-Kobe, Japan July.

[13] Alpatov, A., Cichocki, F., Fokov, A., Khoroshylov, S., Merino, M., and Zakrzhevskii, A., "Determination of the force transmitted by an ion thruster plasma plume to an orbital object," *Acta Astronautica*, Vol. 119, 2016, pp. 241–251.

[14] Sigmund, P., "Theory of sputtering. I. Sputtering yield of amorphous and polycrystalline targets," *Physical review*, Vol. 184, No. 2, 1969, pp. 383.

[15] Matsunami, N., Yamamura, Y., Itikawa, Y., Itoh, N., Kazumata, Y., Miyagawa, S., Morita, K., Shimizu, R., and Tawara, H., "Energy dependence of the ion-induced sputtering yields of monatomic solids," *Atomic Data and Nuclear Data Tables*, Vol. 31, No. 1, 1984, pp. 1–80.

[16] Yamamura, Y. and Tawara, H., "Energy dependence of ion-induced sputtering yields from monatomic solids at normal incidence," *Atomic data and nuclear data tables*, Vol. 62, No. 2, 1996, pp. 149–253.

[17] Zhang, Z. L. and Zhang, L., "Anisotropic angular distribution of sputtered atoms," *Radiation Effects and Defects in Solids*, Vol. 159, No. 5, 2004, pp. 301–307.

[18] Tribble, A. C., Boyadjian, B., Davis, J., Haffner, J., and McCullough, E., "Contamination control engineering design guidelines for the aerospace community," *SPIE's 1996 International Symposium on Optical Science, Engineering, and Instrumentation*, International Society for Optics and Photonics, 1996, pp. 4–15.

[19] Cichocki, F., Merino, M., Ahedo, E., Smirnova, M., Mingo, A., and Dobkevicius, M., "Electric Propulsion Subsystem Optimization for "Ion Beam Shepherd"Missions," *Journal of Propulsion and Power*, 2016/08/28 2016, pp. 0–0.

[20] Yamanaka, K. and Ankersen, F., "New State Transition Matrix for Relative Motion on an Arbitrary Elliptical Orbit," *Journal of guidance, control and dynamics*, Vol. 25, No. 1, 2002, pp. 60–66.